ICEMG 2020-XXXXX

A New PM Halbach Array for Torque Ripple Minimization of Slot-less Axial Flux Wind Turbine Generators

Aghil Ghaheri[1], Akbar Mohammadi Ajamloo[2], Hossein Torkaman[1], Ebrahim Afjei[1]

[1]Faculty of Electrical Engineering, Shahid Beheshti University, Tehran, Iran
[2]Department of Electrical Engineering, K.N.Toosi University of Technology, Tehran, Iran

Abstract

Axial flux permanent magnet machines (AFPMs) are potential candidates for direct-drive wind turbines (DDWTs) due to offering high value of torque density. In slotless AFPM topologies, the cogging torque is absent which makes them more suitable for DDWTs, which provides an easier turbine start-up. In this research, a robust design and optimization procedure of a slotless double-sided AFPM is discussed. The nonlinear magnetic equivalent circuit is established and the optimization is performed by the response surface methodology (RSM) to achieve a cost-effective generator with high power density value. The generator is prototyped and the test results are presented comparing them with the numerical study and non-optimized design results. To minimize the AFPM torque ripple which is necessary for DDWT application, a cost-effective solution is proposed leading to a dramatic improvement in the AFPM torque ripple without reducing the average torque.

Keywords: Axial flux machine, torque ripple, Halbach array, permanent magnet.

Introduction

Recently, the optimum extraction of wind energy has drawn a lot of attention. Consequently, direct-drive turbines are becoming more popular. Owing to the elimination of gearbox, direct-drive wind turbines (DDWTs) offer higher reliability, lower maintenance cost, and higher efficiency in comparison with the geared ones [1]. However, due to the lower speed of DDWTs, the generator of these type of turbines must be designed with high torque density value to reduce the generator volume and weight, resulting in the lower cost of the generator and turbine tower structure [2]. Generally, in wind turbines, the cogging torque and torque ripple of the generators are among the important characteristics and must be as low as possible. Otherwise, the turbine faces trouble during start-up, and heavy vibrations and noise are produced during the spinning [3-5].

In this regard, axial flux permanent magnet machines (AFPMs) are potential alternatives to the radial flux machines for the above-mentioned application. Compared to the radial flux permanent magnet machines (RFPMs), AFPMs are among compact topologies which higher torque densities can be achieved [6-8]. The copper and core weight in AFPM topologies could be reduced significantly, resulting in higher values of efficiency compared to the RFPMs [9]. Moreover, the ratio of machine diameter to

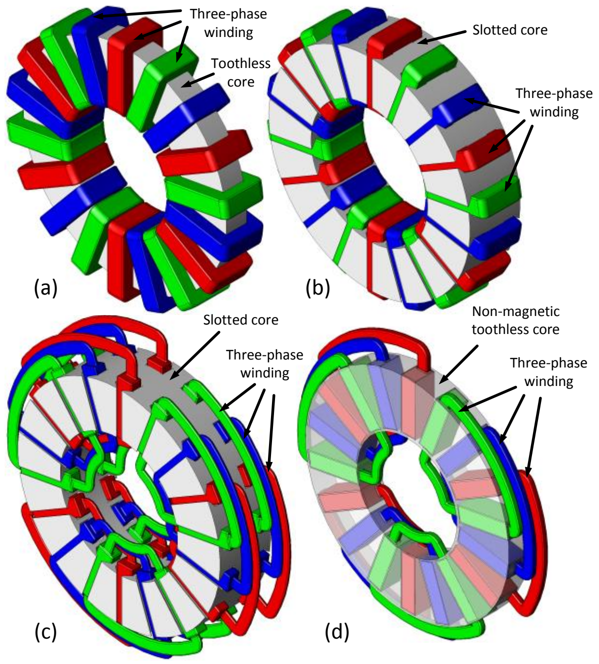

Figure 1. Stator topologies of single stator-double rotor AFPMs. (a) Slotless core with radially wounded coils. (b) Slotted core with radially wounded coils. (c) Slotted core with circumferentially wounded coils. (d) Core-less armature with circumferentially wounded coils.

machine length is high in AFPMs which leads to better heat exchange with the environment [10, 11]. Accordingly, AFPMs are popular in applications with low power ratings that the machine diameter is not too large.

AFPMs can be designed single-sided or double-sided. Applications of single-sided topology is limited because of high attractive force (in the axial direction) between the rotor and the stator and low value of torque density [9]. Consequently, AFPMs are often built double-sided which the axial forces are balanced and the torque density is higher. It is shown that the single stator dual-rotor topology can offer higher torque density than the single rotor dual-stator topology [9, 12]. Hence, this paper focuses on the former topology. Four popular types of stator configurations for such topology are depicted in Fig. 1. According to Fig. 1. (a), the first configuration is composed of a slotless stator iron core and conductors which are wound around it. This stator configuration has the following advantages: 1- Owing to the slotless stator core, the cogging torque is completely absent. 2- The stator core structure is so simple which leads to the easy manufacturing process. 3- The end windings are very short which result in low copper consumption and high value of efficiency [6]. However,

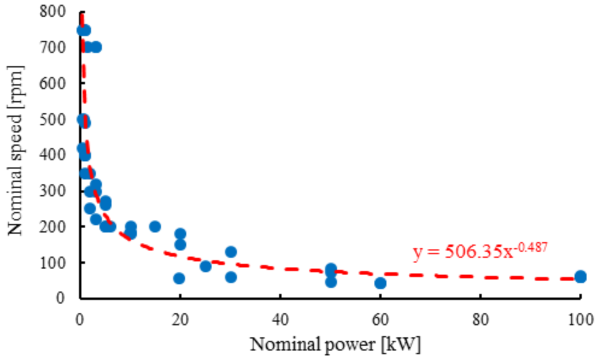

Figure 2. Nominal working point of DDWTs available in market.

the thickness of armature conductors which are placed on the core surface increases the resulting air gap length leading to high PM consumption [13]. The second configuration (Fig. 1. (b)), is the same as the first configuration except the armature core is slotted. In this configuration, the cogging torque is present due to the slotted core. Moreover, the manufacturing process of the stator core is complicated and expensive. However, this configuration has the advantages of small air gap length and low PM consumption [6, 14, 15]. As it can be seen from Fig. 1. (c), the configuration uses the same armature core as the second configuration, but the winding arrangement is different. This topology is only justified on the grounds of having coil pitch equal to one or in the case of single-sided topologies. Otherwise, not only this configuration does not offer any advantages over the second configuration but also has larger end windings which reduces the efficiency and increases the copper consumption [16, 17]. According to Fig. 1. (d), the stator is composed of sets of conductors drowned by epoxy resin or similar materials. This configuration which is known as the coreless stator has two main advantages: Firstly, the cogging torque is absent owing to the coreless armature. Secondly, the manufacturing process of the armature is simple and cheap. However, the absence of the stator iron core increases the resultant air gap length which requires high volume of PMs. Additionally, due to long end windings, the copper loss is high and the efficiency is reduced [18, 19].

In this paper design and analysis of slotless single stator dual-rotor AFPM (Fig. 1. (a)) is addressed. In this topology, the cogging torque is absent which is an outstanding feature in DDWT applications. Unlike the cogging torque, torque ripple is present in this topology which is caused by the interaction between the stator and rotor magneto motive forces (MMFs). As it was mentioned before, the high value of torque fluctuations produces noise and vibrations in the turbine. Moreover, torque ripple hastens blade fatigue failure which reduces turbine's lifetime. Several studies have been presented in the literature addressing torque ripple reduction in AFPMs. Some studies focused on the PMs' shape to improve torque ripple of the AFPMs by using PM skew and PM step skew technique [20, 21]. Furthermore, using sinusoidally and cylindrically shaped PMs instead of the conventional sector-shaped PMs are investigated in [22]. Even though the mentioned methods are effective in reducing the torque ripple, back-EMF reduction and the complicated manufacturing process are the side effects of those methods. Replacing armature conventional rectangular windings with sector-shaped windings can help in the reduction of torque ripple in slotless AFPMs [20, 23]. However, the solution does not have a major impact on the torque ripple reduction, and it increases machine copper loss. Using the Halbach array of PMs can be adapted to minimize the torque ripple of slotless AFPMs. Since the torque ripple is highly dependent on the Halbach PM coverage and orientation, sensitivity analyses could be performed to choose the optimum PM coverage [24]. Unlike the above-mentioned solutions, not only using Halbach PMs does not deteriorate machine performance but also improves its performance by increasing the average torque and back-EMF [25].

In this paper, design procedure of the slotless single stator dual-rotor AFPM is presented and a conventional slotless AFPM is designed and prototyped. In order to reduce the torque ripple and improve the voltage THD, segmented Halbach-Array is proposed, sensitivity analyzes is performed, and compared with the conventional Halbach PMs. Moreover, the experimental setup of conventional AFPM is given and machine characteristics are discussed. At the end, a comparative study is presented helping to a better assessment of the AFPM topologies discussed in this paper.

Analytical Design of AFPM Generator for DDWT

In this section, the requirements of DDWT generators is addressed and design formulation of the slotless single stator dual-rotor AFPM is discussed. The double sided slotless AFPM configuration consists of two rotor discs and one stator core. The configuration is also called N-N type TORUS AFPM in which the similar rotor poles of the two rotor disks face each other. The stator core is made of continues steel tape and the windings are wound around the stator core.

Generally, wind turbines are categorized into horizontal axis wind turbines (HAWTs) and vertical axis wind turbines (VAWTs). HAWTs benefit from higher efficiency in comparison with the VAWTs. Moreover, the HAWTs can be installed in higher heights which the high speed winds are available. However, the VAWTs have some advantages over the HAWTs like lower maintenance cost and lower acoustic noise. In this study, HAWTs are selected since they have more annual energy yield than VAWTs. The power equation of wind turbine could be written as in (1);

$$P_T = \frac{1}{2} C_p A_w V^3 \tag{1}$$

where A_w is blades swept area, V is the velocity of the wind, and C_p is the power coefficient of the turbine which obtains the values less than 59.3% according to Betz limit. The value of power coefficient depends on the blade pitch angle and the tip speed ratio (TSR) which is defined as in below;

$$\lambda = \frac{\omega_r R}{V} \tag{2}$$

Here, ω_r and R are the angular velocity of the turbine and blade radius; respectively.

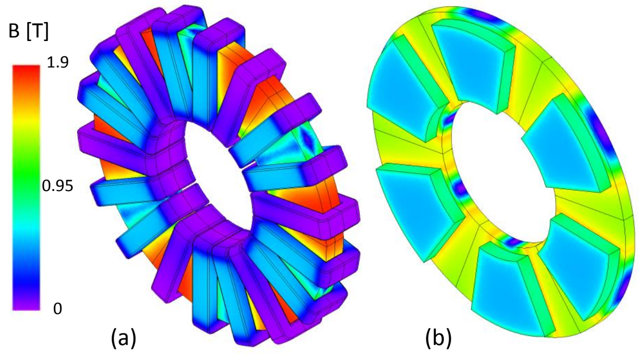

Figure 3. Magnetic flux density distribution in the AFPM (a) stator, (b) one rotor disc.

Wind turbines must be utilized at a certain TSR (generally around 7 for HAWTs with 3 blades) to attain the maximum power coefficient. Thus, let assume that the wind speed (V) is constant, therefore according to (1), the turbine power is proportional to the blades swept area (or square blade radius (R_2)). Thus, to have a turbine with a higher power rate, the turbine blade radius must be increased. On the other hand, according to (2), to keep the TSR at its optimum value, the angular velocity of the turbine must be inversely proportional to the blade radius. Consequently, wind turbines nominal power and speed are related as in (3).

$$\omega_r \propto P_T^{-0.5} \tag{3}$$

In other words, wind turbines with higher power ratings work at lower speeds. The nominal working point of the various direct-drive wind turbines which are available in the market are extracted and presented in Fig. 2. As it could be seen, the power rating of the wind turbines is inversely proportional to their speed. In this paper, a 1.2 kW HAWT with the nominal speed of 500 rpm is selected and the AFPM is designed as its direct drive generator.

According to [6], the electromagnetic torque (Te) of the understudy AFPM could be written as in (4);

$$T_e = \frac{\pi}{8}\alpha_i k_w k_s B_{mg} A_m D_o^3 (1-k_d^2)(1+k_d)\cos(\varphi) \tag{4}$$

where α_i, k_w, k_s, B_{mg}, A_m, D_o, k_d , and $\cos(\varphi)$ are pole width (coverage) to pole pitch ratio, winding factor, stacking factor, maximum magnetic field in air gap, electrical loading per stator active surface, machine outer diameter, the ratio of machine inner diameter to outer diameter, and power factor, respectively.

The RMS value of induced winding voltage (E_f) is calculated as in (5) [6];

$$E_f = \frac{\sqrt{2}\pi^2}{4}\alpha_i k_w k_s N_1 B_{mg} D_o^2 (1-k_d^2) n_s \tag{5}$$

where N_1 and ns are number of coil turns per phase in the stator active surface and the rotor speed in rps, respectively.

The resultant value of air gap length is the sum of mechanical clearance between the rotor and the stator poles and the coil length. The coil length (L_w) is calculated as in (6);

$$L_w = \frac{3N_1 d_w^2}{2k_f D_i} \tag{6}$$

where d_w, k_f, and D_i are the diameter of each conductor, winding fill factor, and machine inner diameter, respectively.

To calculate the required PM length, Ampere's law is applied on the main magnetic flux path as in (7) and the PM length is calculated as in (8);

$$2H_m L_m + 2H_g(L_g + L_w) + V_{stator} + V_{rotor} = 0 \tag{7}$$

$$L_m = \frac{\mu_r B_{mg}(L_g + L_w) + 0.5\mu_0\mu_r(V_{stator} + V_{rotor})}{B_r - \dfrac{B_{mg}}{k_{pm}}} \tag{8}$$

where H_m and H_g are magnetic field strength of PM and resultant air gap, respectively. μ_r, L_g, and B_r are relative permeability of PM, mechanical clearance between the rotor and the stator, and PM remanent flux density, respectively. V_{stator} and V_{rotor} are magnetic potential drop in the main flux path of the rotor and the stator iron parts, and k_{pm} is the ratio of axial component of air gap flux to total flux produced by PMs. Armature copper loss of the AFPM is calculated as in (9), where r is the conductor resistance per meter, I_a is the RMS value of armature current, and L_{ave} is the average length of each winding turn.

$$P_{cu} = 6rN_1 L_{ave} I_a^2 \tag{9}$$

The magnetic flux density of the stator iron yoke is calculated as in (10). The iron loss is determined by (11) which L_{yoke} and ρ_{iron} are the axial length of armature iron core and iron density, f_e is the electrical frequency, k_{fe} is the correction factor of iron loss [26] and P (1.5, fe) is the specific loss of the iron core (W/kg) at flux density of 1.5 T and frequency of fe.

$$B_{yoke} = \alpha_i B_{mg} \frac{\pi D_o(1+k_d)}{4pL_{yoke}} \tag{10}$$

$$P_{iron} = \frac{\pi D_o^2(1-k_d^2)}{4} L_{yoke}\ \rho_{iron} P_{(1.5,\, f_e)} k_{fe} \left(\frac{B_{yoke}}{1.5}\right)^2 \tag{11}$$

The Prototyped Conventional AFPM Generator

The design procedures of the AFPM for a 1.2 kW DDWT were presented. Accordingly, the AFPM is designed and its specifications are given in table 1. Then, the FEM is carried out to verify the design procedure of the AFPM. In Fig. 3, the contour plot of the magnetic flux density distribution in the AFPM is presented. The results show that magnetic flux density in stator iron yoke reaches the iron B-H curve knee

Table 1. Specifications of the designed AFPM.

Parameter	symbol	Value	Unit
Rated power	P_{out}	1.2	kW
Rated speed	n_m	500	rpm
No. of phases	m	3	---
No. of poles	p	6	---
No. of armature coils	n_{coil}	18	---
Machine outer diameter	D_o	220	mm
Machine inner diameter	D_i	113.6	mm
Machine length	L	77	mm
Air gap length	L_g	1	mm
PM coercive force (20°C)	H_c	-896	kA/m
PM remanent flux density (20°C)	B_r	1.21	T

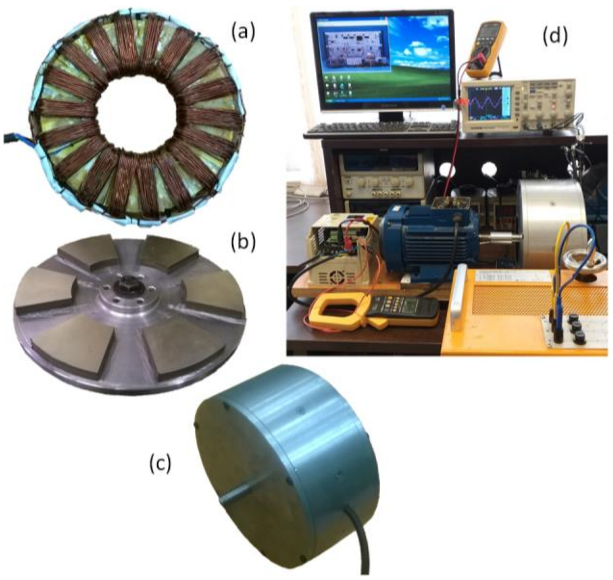

Fig. 4. AFPM configuration and the test setup. (a) stator, (b) one rotor disk, (c) assembled AFPM, (d) test setup.

point (1.7 T) while the magnetic flux density is about 1.4 T in the rotor yoke. Even though in double-sided AFPMs, axial forces are balanced, each rotor disk experiences high axial force which tends to bend it toward the stator core. So, the rotor disk should be thick enough to withstand such attractive force and maintain the uniform air gap length. Consequently, rotor yoke thickness is mainly determined by mechanical considerations rather than the iron saturation effect.

The prototyped AFPM along with its component and the provided setup test are presented in Fig. 3. The stator core shown in Fig. 4 is made of a twisted continues electrical steel tape with a thickness of 0.5 mm. After insulating the stator core, 18 coils are wound around the core which is shown in Fig. 4 (a). One of the rotor disks is also shown in Fig. 4 which is composed of a single solid iron yoke and six specially shaped NdFeB PMs glued on the iron yoke.

The measured and simulated (FEM) induced line voltage of the AFPM are presented in Fig. 5. As it could be seen, the FEM results have acceptable adaption to the experimental results. Furthermore, in Fig.6, terminal voltage of the generator at different currents is measured and compared with the simulation results. Two load types are considered for the test: pure resistive load and resistive-capacitive load (0.9 lead). The results indicate that increasing the armature current does not affect the

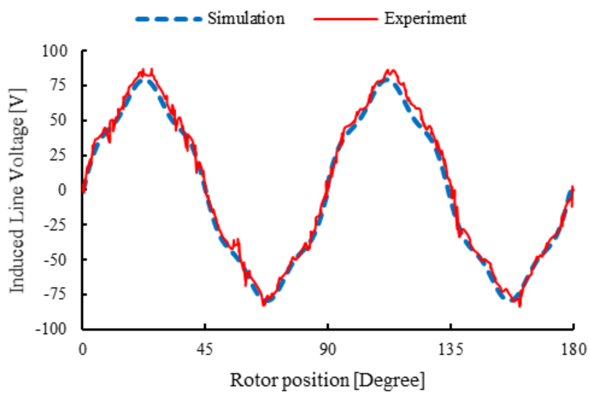

Fig. 5. Induced line voltage waveform of the AFPM.

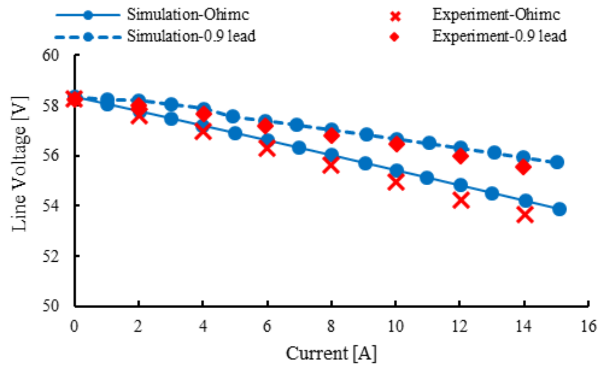

Fig. 6. Terminal line voltage of the AFPM at different resistive and resistive-capacitive (0.9 lead) loads.

terminal voltage substantially as the voltage drop is less than 10% in the resistive load. In the case of the resistive-capacitive load, the voltage drop is even lower and is less than 4%. Regarding Fig. 6, the simulation results have a good level of accuracy since the maximum error is less than 3% in the worst case which is mainly because of the manufacturing tolerances. The electromagnetic torque waveform of the AFPM is extracted at the nominal resistive load and presented as the black line in Fig. 7. It is seen that the generator average torque got the value of 23.85 N.m and the torque ripple is 15%. As it could be noticed from Fig. 7, the generator (regular AFPM) suffers from high values of torque ripple (15%) which is not suitable for DDWT application. Aiming to minimize the generator torque fluctuations, using a new arrangement of Halbach PMs is proposed and studied in the next section.

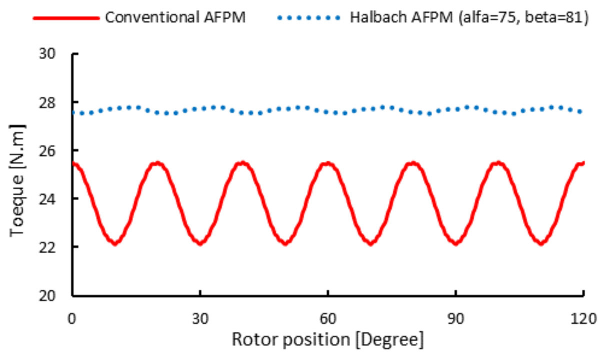

Fig. 7. Electromagnetic torque waveform of the conventional and proposed Halbach AFPM at rated load.

The Proposed Halbach Array

According to the above discussions, the torque ripple of the generator is almost 15%. In DDWT application, high values of the torque ripple increases the vibrations which cause fatigue to the blades and increases the acoustic noises. Hence, this paper proposes using the new Halbach-array of PMs to minimize the torque ripple of the AFPM. Unlike the conventional configuration of PMs which are magnetized only in the axial direction, in the case of Halbach configuration, the PMs are magnetized in multiple directions. Depending on the number of magnetization directions (k), k-segmented Halbach arrays are developed in which there are k pieces of PMs per pole. However, increasing the number of PMs per pole complicates the manufacturing process.

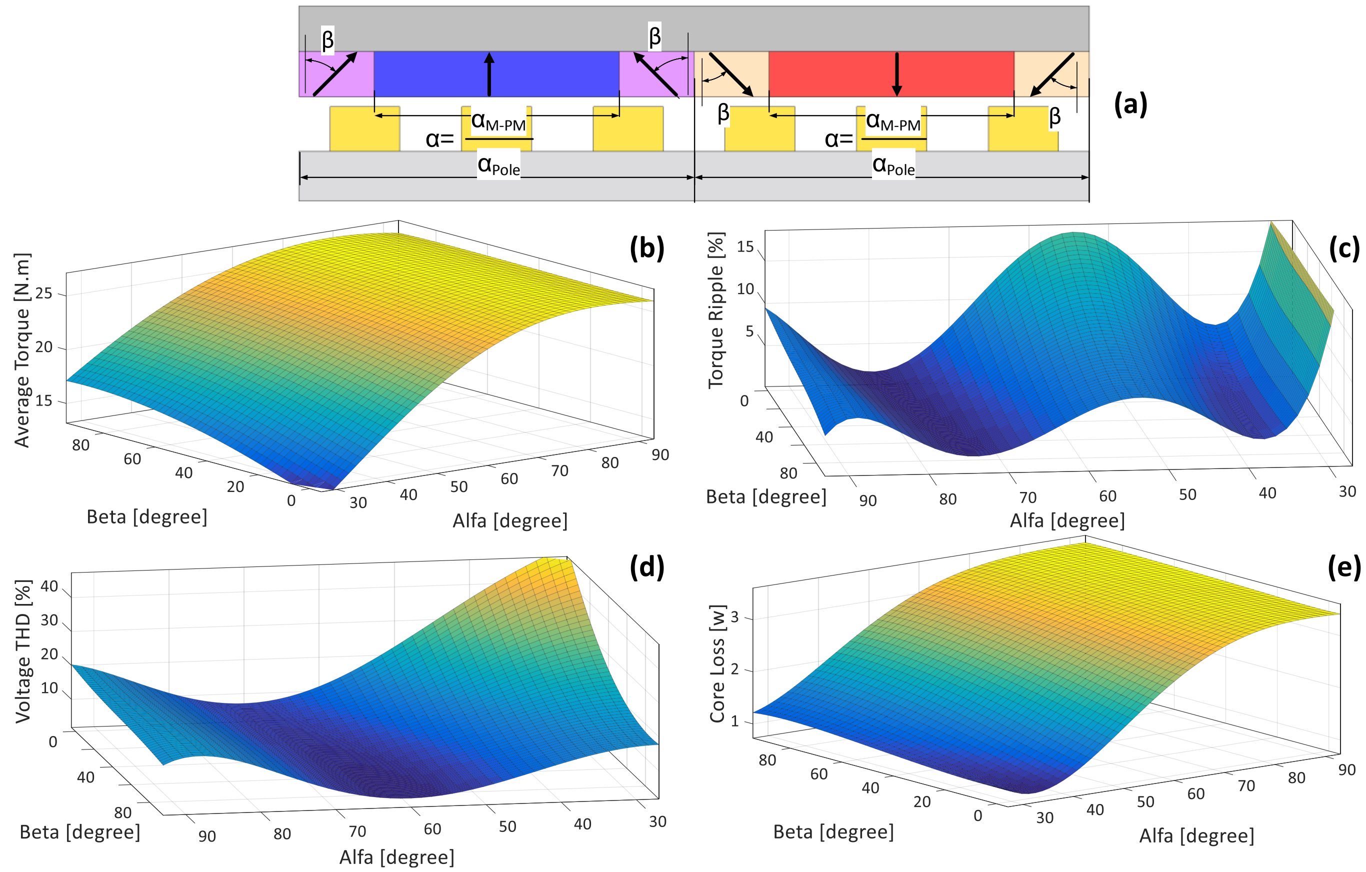

Figure 8. The proposed AFPM and the corresponding characteristics at different Halbach PM angles. (a) the proposed Halabach array configuration (b) average torque, (c) torque ripple, (d) voltage THD, (e) core loss.

Moreover, it also requires magnetization of the PMs in more directions which increases the manufacturing cost. In this study, three-segmented Halbach-array is selected and the designed generator is adjusted by only substituting the PMs as in Fig. 8 (a). As it could be seen, there are two types of PMs per pole. The first one is the main PM and is magnetized in the axial direction while the other are magnetized non-radially and called the side PMs. In the regular Halbach configurations, NdFeB PMs are used as both of the main and side PMs. Here, the ratio of main PM coverage to the pole pitch (alfa), and the side PMs' magnetization angle (beta) are taken as two key variable parameters to be optimized. These parameters are varied between and the machine parameters are extracted and presented in Fig. 8(b)-(d). It should be note that torque characteristics of are extracted at the constant load (rated current) in the entire analysis. From Fig. 8 (c), it is seen that the torque ripple of the generator has an extremely nonlinear behavior. According to Fig. 8 (c), the torque ripple of the generator could be reduced to 0.9% by choosing either combinations of (alfa=38%, beta=88%) and (alfa=75%, beta=81%). Moreover, from Fig. 8 (b) it is noticed that the electromagnetic torque of the generator is mostly dependent to the parameter alfa. In this regard, higher average torque is produed at high values of the parameter alfa. Consequently, in order to achive the minimum value of the torque ripple and enhance the machine average torque, the second combination of parameters should be selected (alfa=75%, beta=81%). In order to have more insight into the machine parameters, the voltage total harmonic distortion (THD) and the core loss in different parameter values are presented in Fig. 8 (d) and € respectively. Accordingly, by choosing the above-mentioned combination, the machine voltage THD and core loss are 8.4% and 2.6 w respectively.

Based on above-mentioned points, in order to reach the goal of the study which is minimizing the torque ripple, the value of alfa and beta must be set at 75% and 81% respectively. Accordingly, the torque waveform of the Halbach-array AFPM is extracted by using FEM and presented in Fig. 7. As it could be seen both the average torque and torque ripple have improved significantly. Compared to the basic design, the average torque has reached from 23.85 N.m to 27.8 N.m. Moreover, the torque ripple has dropped from 15% to 0.9%. It is noteworthy to mention that at the aforementioned combination, compared to the basic design, the phase voltage THD has increased from 4.9% to 10.5% which is a side effect of the proposed Halbach arrangement.

Conclusion

In this paper, a 1.2 kW AFPM generator is designed for a 500 rpm DDWT. The generator is prototyped and the comparison is made between the experimental and simulation results. The comparison shows a high level of adaption between these results. In order to minimize the torque ripple of the generator which is troublesome in DDWTs, using a new Halbach PM array is investigated and a sensitivity analysis is carried out to select the optimum array. A comparison is also made between the AFPM topologies which reveals that torque ripple of the generator reduces from 15% to 0.9% by using the optimum Halbach. Furthermore, the average torque increase by 16.5%. Consequently, the proposed Halbach AFPM could be considered as a potential candidate for DDWT application.

References

[1] A. McDonald and N. A. Bhuiyan, "On the optimization of generators for offshore direct drive wind turbines," *IEEE Transactions on Energy Conversion,* vol. 32, pp. 348-358, 2017.

[2] R. Nasiri-Zarandi, A. M. Ajamloo, and K. Abbaszadeh, "Proposing the Output Equations and 3-D MEC Modeling for U-Core TFPM Generators," *2018 International Symposium on Power Electronics, Electrical Drives, Automation and Motion (SPEEDAM),* pp. 292-297, 2018.

[3] T. Husain, I. Hasan, Y. Sozer, I. Husain, and E. Muljadi, "Design considerations of a transverse flux machine for direct-drive wind turbine applications," *IEEE Transactions on Industry Applications,* 2018.

[4] J. R. Vaz, D. H. Wood, D. Bhattacharjee, and E. F. Lins, "Drivetrain resistance and starting performance of a small wind turbine," *Renewable energy,* vol. 117, pp. 509-519, 2018.

[5] R. Nasiri-Zarandi, A. Ghaheri, and K. Abbaszadeh, "Cogging Torque Reduction in U-Core TFPM Generator Using Different Halbach-Array Structures," in *2018 International Symposium on Power Electronics, Electrical Drives, Automation and Motion (SPEEDAM)*, 2018, pp. 1153-1158.

[6] J. F. Gieras, R.-J. Wang, and M. J. Kamper, *Axial flux permanent magnet brushless machines*: Springer Science & Business Media, 2008.

[7] H. Torkaman, A. Ghaheri, and A. Keyhani, "Design of rotor excited axial flux-switching permanent magnet machine," *IEEE Transactions on Energy Conversion,* vol. 33, pp. 1175-1183, 2018.

[8] H. Torkaman, A. Ghaheri, and A. Keyhani, "Axial flux switched reluctance machines: a comprehensive review of design and topologies," *IET Electric Power Applications,* vol. 13, pp. 310-321, 2019.

[9] Y. Chen, P. Pillay, and A. Khan, "PM wind generator comparison of different topologies," *Conference Record of the 2004 IEEE Industry Applications Conference, 2004. 39th IAS Annual Meeting.,* vol. 3, pp. 1405-1412, 2004.

[10] A. Daghigh, H. Javadi, and H. Torkaman, "Design optimization of direct-coupled ironless axial flux permanent magnet synchronous wind generator with low cost and high annual energy yield," *IEEE transactions on magnetics,* vol. 52, pp. 1-11, 2016.

[11] C. L. Sabioni, M. F. Ribeiro, and J. A. Vasconcelos, "Robust design of an axial-flux permanent magnet synchronous generator based on many-objective optimization approach," *IEEE Transactions on Magnetics,* vol. 54, pp. 1-4, 2018.

[12] A. Mahmoudi, H. W. Ping, and N. A. Rahim, "A comparison between the TORUS and AFIR axial-flux permanent-magnet machine using finite element analysis," *2011 IEEE International Electric Machines & Drives Conference (IEMDC),* pp. 242-247, 2011.

[13] M. Baghayipour, A. Darabi, and A. Dastfan, "Detailed analytical method for predicting the steady-state time variations and entire harmonic contents of principal performance characteristics in a non-slotted axial flux permanent magnet motor, considering a precise iron loss model," *IET Electric Power Applications,* vol. 12, pp. 308-322, 2017.

[14] L. Xiao, J. Li, R. Qu, Y. Lu, R. Zhang, and D. Li, "Cogging torque analysis and minimization of axial flux PM machines with combined rectangle-shaped magnet," *IEEE Transactions on Industry Applications,* vol. 53, pp. 1018-1027, 2017.

[15] A. Mahmoudi, S. Kahourzade, N. A. Rahim, and W. P. Hew, "Design, analysis, and prototyping of an axial-flux permanent magnet motor based on genetic algorithm and finite-element analysis," *IEEE Transactions on Magnetics,* vol. 49, pp. 1479-1492, 2013.

[16] C.-W. Kim, G.-H. Jang, J.-M. Kim, J.-H. Ahn, C.-H. Baek, and J.-Y. Choi, "Comparison of axial flux permanent magnet synchronous machines with electrical steel core and soft magnetic composite core," *IEEE Transactions on Magnetics,* vol. 53, pp. 1-4, 2017.

[17] N. Taran, V. Rallabandi, G. Heins, and D. M. Ionel, "Coreless and conventional axial flux permanent magnet motors for solar cars," *IEEE Transactions on Industry Applications,* vol. 54, pp. 5907-5917, 2018.

[18] S. Neethu, S. P. Nikam, S. Singh, S. Pal, A. K. Wankhede, and B. Fernandes, "High-Speed Coreless Axial-Flux Permanent-Magnet Motor With Printed Circuit Board Winding," *IEEE Transactions on Industry Applications,* vol. 55, pp. 1954-1962, 2019.

[19] J. Zhu, S. Li, D. Song, Q. Han, J. Wang, and G. Li, "Multi-objective optimisation design of air-cored axial flux PM generator," *IET Electric Power Applications,* vol. 12, pp. 1390-1395, 2018.

[20] M. Aydin, S. Huang, and T. A. Lipo, "Torque quality and comparison of internal and external rotor axial flux surface-magnet disc machines," *IEEE transactions on industrial electronics,* vol. 53, pp. 822-830, 2006.

[21] S. J. Arand and M. Ardebili, "Cogging torque reduction in axial-flux permanent magnet wind generators with yokeless and segmented armature by radially segmented and peripherally shifted magnet pieces," *Renewable energy,* vol. 99, pp. 95-106, 2016.

[22] M. Shokri, N. Rostami, V. Behjat, J. Pyrhönen, and M. Rostami, "Comparison of performance characteristics of axial-flux permanent-magnet synchronous machine with different magnet shapes," *IEEE Transactions on Magnetics,* vol. 51, pp. 1-6, 2015.

[23] M. R. Pahlavani, Y. S. Ayat, and A. Vahedi, "Minimisation of torque ripple in slotless axial flux BLDC motors in terms of design considerations," *IET Electric Power Applications,* vol. 11, pp. 1124-1130, 2017.

[24] I. P. Wiltuschnig, P. R. Eckert, D. G. Dorrell, and A. F. Flores Filho, "A Study of the Influence of Quasi-Halbach Arrays on a Torus Machine," *IEEE Transactions on Magnetics,* vol. 52, pp. 1-4, 2016.

[25] W. Geng and Z. Zhang, "Analysis and Implementation of New Ironless Stator Axial-Flux Permanent Magnet Machine With Concentrated Nonoverlapping Windings," *IEEE Transactions on Energy Conversion,* vol. 33, pp. 1274-1284, 2018.

[26] J. Pyrhonen, T. Jokinen, and V. Hrabovcova, *Design of rotating electrical machines*: John Wiley & Sons, 2013.